Chinese Journal of Aeronautics 24 (2011) 1-7

Contents lists available at ScienceDirect

Chinese Journal of Aeronautics

journal homepage: www.elsevier.com/locate/cja

Numerical Simulation of Unsteady Flow Around Forward Flight Helicopter with Coaxial Rotors

XU Heyong, YE Zhengyin*

National Key Laboratory of Science and Technology on Aerodynamic Design and Research, Northwestern Polytechnical University, Xi'an 710072, China

Received 19 April 2010; revised 20 May 2010; accepted 5 July 2010

Abstract

Three-dimensional unsteady Euler equations are numerically solved to simulate the unsteady flows around forward flight helicopter with coaxial rotors based on unstructured dynamic overset grids. The performances of the two coaxial rotors both become worse because of the aerodynamic interaction between them, and the influence of the top rotor on the bottom rotor is greater than that of the bottom rotor on the top rotor. The downwash velocity at the bottom rotor plane is much larger than that at the top rotor plane, and the downwash velocity at the top rotor plane is a little larger than that at an individual rotor plane. The downwash velocity and thrust coefficient both become larger when the collective angle of blades is added. When the spacing between the two coaxial rotors increases, the thrust coefficient of the top rotor increases, but the total thrust coefficient reduces a little, because the decrease of the bottom rotor thrust coefficient is larger than the increase of the top rotor thrust coefficient.

Keywords: coaxial rotors; unstructured grid; overset grids; thrust coefficient; interaction flow; helicopters; numerical simulation

1. Introduction

Coaxial rotors configuration is one of the technological solutions for increasing helicopter load-carrying ability. Since two rotors produce the net thrust instead of a single rotor in the conventional design, the diameter of the rotors can be reduced to carry the same amount of weight. The most attractive feature of a coaxial design is the resulting compactness and safety of the vehicle. Secondly, the converse torsional moments generated by the two rotors would be canceled due to the opposite rotational directions, and the tail rotor and tail boom can be eliminated, resulting in a smaller and lighter vehicle.

Compared to the individual rotor helicopter, the aerodynamics and flow physics of coaxial rotor helicopter are relatively less studied and understood. The method of slipstream theory was firstly used to study the coaxial rotors, and then the predicted wake vortex model[1-2], free wake vortex model[3], momentum theory[4], and blade-element momentum theory(BEMT)[5-6] were applied to the coaxial rotor analysis. Recently, the unsteady Euler/Navier-Stokes equations based on structured overset grids were used to simulate the time-accurate flows around coaxial rotors[7-9]. In our nation, some researchers have used methods of momentum source terms[10-11], rigid-wake mode[12], experimental data analysis[13], and free-vortex wake model[14] to investigate the property of coaxial rotors. Except the time-accurate unsteady simulation method,

*Corresponding author. Tel.: +86-29-88491374.
E-mail address: yezy@nwpu.edu.cn
Foundation items: China Postdoctoral Science Foundation (20100481368); National Key Laboratory Foundation of China

doi: 10.1016/S1000-9361(11)60001-0

the other methods above all carried out some approximations to the rotor, and the detailed flow feature near the blades and blade vortex in the wake could not be simulated, and the solutions were just time-averaged. In the previous study, Xu, et al. investigated the aerodynamics of the coaxial rotor helicopter in hover by solving the unsteady Euler equations based on unstructured dynamic overset grids[15]. At present, studies of time-accurate numerical simulation of the forward flight coaxial rotor helicopter have not been found in the open literature domestically.

In the present article, three-dimensional unsteady Euler equations are solved to simulate the forward flight flow around coaxial rotor helicopter based on the unstructured dynamic overset grids. The aerodynamic interaction property of the coaxial rotor helicopter in forward flight, and the influence of some parameters on the coaxial rotor performance are investigated fairly detailedly.

2. Unstructured Overset Grid Generation

For the lack of the standard model of coaxial rotor helicopter, here we use an assembled model. The fuselage model of the NASA (National Aeronautics and Space Administration) ROBIN (ROtor-Body INteraction) configuration is used for the coaxial rotor helicopter's fuselage, and the coaxial rotors are two-layer four-blade rotors. The ROBIN fuselage has an analytical configuration, and the coordinates of the ROBIN body are defined by super-ellipse equations. For a given non-dimensional body longitudinal station, the non-dimensional coordinates of the cross section are obtained from the analytic functions for the model height, width, camber and elliptical power, and Ref.[16] gives the detailed analytic functions. The blades are made of an NACA (National Advisory Committee for Aeronautics) 0012 airfoil section and have a rectangular planform shape with an aspect ratio of 12.98. The root cutout is at 24% of the radius. The blades have no linear twist and the forward tilt angle of rotor shaft is 0°.

The two-layer rotors rotate at converse directions with a high velocity when the coaxial rotors are on working. For the effective treatment of the complicated flow field involving the relative motion between the blades and the fuselage, the computational domain is decomposed into three subzones. The two rotational subzones contain the top and bottom rotors respectively, and rotate with them. The stationary subzone covers the remainder of the flow field including the fuselage and the far wake of the rotor.

After grid generation, we can obtain the unstructured overset grids for the coaxial rotor helicopter configuration, containing three subzone meshes, as shown in Fig.1. The slice meshes of the top rotor subzone and bottom subzone and fuselage subzone are shown in Figs.1(a)-(c) respectively, and the overlapping drawing of the slice meshes is shown in Fig.1(d). The procedure of generating unstructured overset grids was given detailedly in Refs.[17]-[18]. This method can ensure that there is always a reasonable overlapping area between overset subzones at every time stepping during the unsteady simulation, without any hole boundary regeneration and inverse map grid generation, which increases the efficiency of generating overset grids and unsteady simulation.

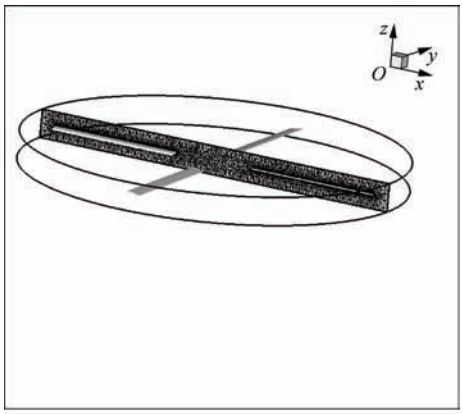

(a) Slice meshes of top rotor subzone

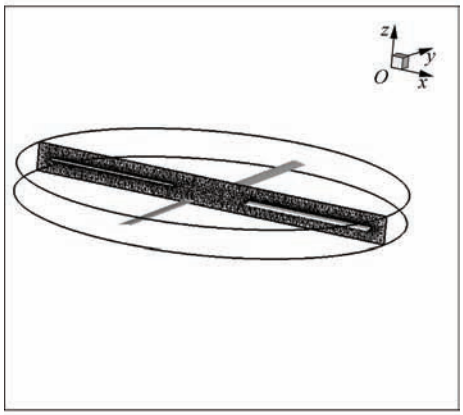

(b) Slice meshes of bottom rotor subzone

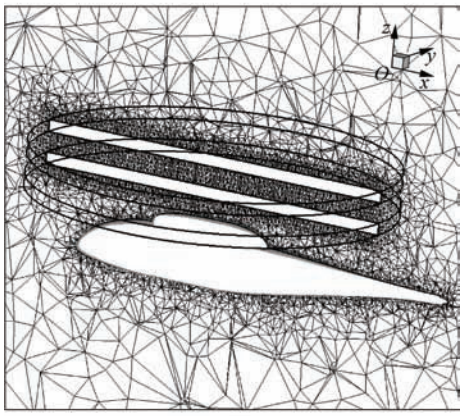

(c) Slice meshes of fuselage subzone

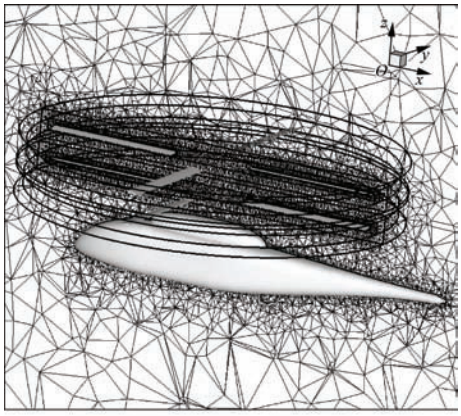

Fig.1 Overset grids of coaxial rotors helicopter.

3. Numerical Method

3.1. Governing equation

The unsteady Euler equations in an arbitrary lagrangian Eulerian (ALE) formulation[19] are discretized by a centre finite-volume method on the inertial coordinate system. The integral form of unsteady Euler equations for a bounded domain Ω with a boundary $\partial\Omega$ can be written as

$$\frac{\partial}{\partial t}\iiint_{\Omega}\boldsymbol{Q}\mathrm{d}V+\iint_{\partial\Omega}\boldsymbol{F}(\boldsymbol{Q})\cdot\boldsymbol{n}\mathrm{d}S=\boldsymbol{0} \tag{1}$$

where $\boldsymbol{Q}=[\rho\ \ \rho u\ \ \rho v\ \ \rho w\ \ e_0]^{\mathrm{T}}$, and $\boldsymbol{F}(\boldsymbol{Q})$ is the inviscid flux vector and $\boldsymbol{n}$ is the exterior surface unit normal vector on the boundary. Variables ρ and e_0 are the density and total energy per unit volume, respectively. u, v and w are the velocities in x, y and z(downwash velocity) axes, and they are non-dimensionalized by the sonic velocity of incoming flow. The inviscid flux across each cell face is computed based on the Jameson's central difference scheme. To obtain second-order spatial accuracy, estimation of the state variables at each cell face is achieved by interpolating the solution using the Taylor series expansion in the neighborhood of each cell center. The cell-averaged solution gradient required at the cell center for the above expansion is computed from the Gauss' theorem by evaluating the surface integral for the closed surface of the tetrahedron. The expansion also requires the nodal value of the solution, which can be computed from the surrounding cell center data using a second-order accurate pseudo-Laplacian averaging procedure.

3.2. Time stepping

A dual-time stepping[20] is adopted to advance the time-accuracy solution in time for the ith volume element as follows:

$$\frac{\mathrm{d}}{\mathrm{d}\tau}(\boldsymbol{Q}_i^{n+1}V_i^{n+1})+\boldsymbol{R}^*(\boldsymbol{Q}_i^{n+1})=\boldsymbol{0} \tag{2}$$

$$\boldsymbol{R}^*(\boldsymbol{Q}_i^{n+1})=\frac{3\boldsymbol{Q}_i^{n+1}V_i^{n+1}-4\boldsymbol{Q}_i^{n}V_i^{n}+\boldsymbol{Q}_i^{n-1}V_i^{n-1}}{2\Delta t}+\boldsymbol{R}(\boldsymbol{Q}_i^{n+1}) \tag{3}$$

where τ is the pseudo time, Δt the scale of real time-stepping, V_i^n the volume of grid element at time level n, $\boldsymbol{R}(\boldsymbol{Q}_i^{n+1})$ the residual in pseudo timestepping, and $\boldsymbol{R}^*(\boldsymbol{Q}_i^{n+1})$ the residual in real timestepping. An explicit multi-stage timestepping scheme is used to discretize the time derivative in Eq.(2). The solution is advanced from time t to $t+\Delta t$ with a four-stage Runge-Kutta scheme[21], given by

$$\left.\begin{aligned}&\boldsymbol{W}^{(0)}=(\boldsymbol{W}^{*})_t\\&\boldsymbol{W}^{(i)}=\boldsymbol{W}^{(0)}-\alpha_j\Delta\tau\boldsymbol{R}^*(\boldsymbol{W}^{(i-1)})\\&(\boldsymbol{W}^{*})_{t+\Delta t}=\boldsymbol{W}^{(4)}\end{aligned}\right\} \tag{4}$$

where j = 1,2,3,4 is the stage counter for the four-stage scheme and α_j is the multi-stage coefficient for the jth stage with values being 1/4,1/3,1/2 and 1 respectively in this article.

4. Results and Discussion

4.1. Simulation of coaxial rotors in hover

The validation of the present method for predicting forward flight flow around coaxial rotor helicopter is made for the coaxial rotor model in hover, which is experimented in Japan in the late 1970s[22]. The hover state is considered as a special forward flight, namely the advancing ratio is zero. The blades have an NACA 0012 airfoil section with no twist angle, and the calculation model has no fuselage. The parameters of coaxial rotors are shown in Table 1.

Table 1 Parameters of experimental coaxial rotors

Name of parameter	Symbol	Value
Radius of rotors	R/m	0.38
Rotor spacing	H/m	0.10
Airfoil chord	c/m	0.06
Root cutout	r_c/%	21
Rotational speed	ω/(rad·s^{-1})	324.5
Collective angle	θ/(°)	3-12

The slice meshes of the unstructured overset grids are shown in Fig.2. After a series of unsteady calculations, the variation of thrust coefficient C_T with torque coefficient C_Q is shown in Fig.3, and they have a fairly good agreement with the experimental data, which demonstrates that the present method is effective and accurate for the prediction of unsteady flow around coaxial rotors.

From Fig.3, we can find that the thrust of top rotor is larger than that of the bottom rotor for the same torque coefficient, due to the aerodynamic interaction between the two rotors. For the bottom rotor, the wake vortex of the top rotor directly traverses through the bottom rotor plane into its wake vortex, and the downwash is the collective effect of the two rotors, which results in decreasing the effective angle of attack of the bottom rotor. So the thrust of the bottom rotor is smaller than that of the top rotor.

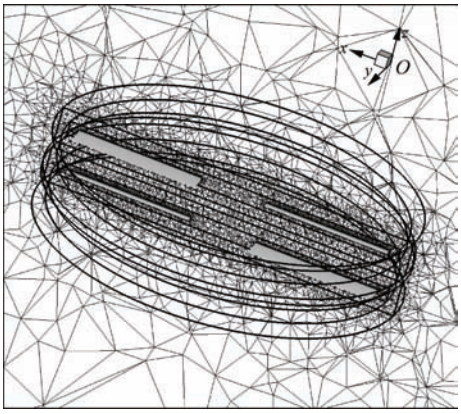

Fig.2 Overset grids of coaxial rotors.

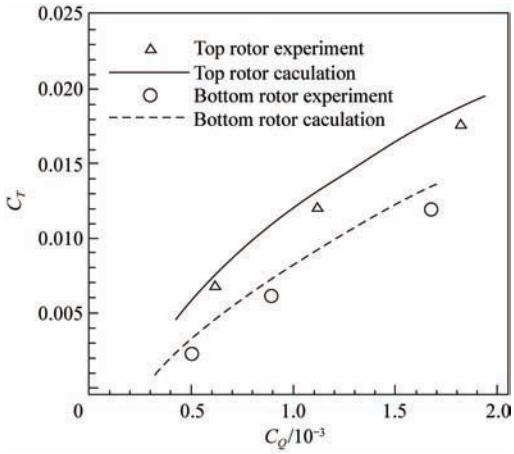

Fig.3 Comparison of C_T-C_Q curves in experiment and calculation.

4.2. Simulation of forward flight coaxial rotor helicopter

The unsteady flow around forward flight coaxial rotor helicopter is simulated to investigate the aerodynamic interaction among the two rotors and fuselage. The parameters of calculation are shown detailedly in Table 2. For the comparison between coaxial rotor helicopter and individual rotor helicopter, unsteady flow around an individual rotor helicopter is also simulated, and the configuration of the individual rotor helicopter is just the coaxial rotor helicopter configuration with the top rotor removed.

Table 2 Parameters of calculational coaxial rotor helicopter

Name of parameter	Symbol	Value
Advancing ratio	μ	0.03
Radius of rotor	R/m	0.86
Rotor spacing	H/m	0.16
Tip Mach number	M_t	0.52
Shaft tilting angle	α_s/(°)	0
Attack angle	α/(°)	0
Coning angle	β/(°)	0
Longitudinal flapping angle	β_1/(°)	0
Lateral flapping angle	β_2/(°)	0
Collective angle	θ/(°)	8
Longitudinal pitching angle	θ_1/(°)	0
Lateral pitching angle	θ_2/(°)	0

The thrust coefficients of coaxial rotors and individual rotor varying with azimuth angle ψ are given in Figs.4-5, and after the second period, the results present to be steady-going periodic solutions. For the coaxial rotors, the thrust of top rotor is larger than that of bottom rotor, while the thrust of individual rotor is a little larger than that of the top rotor. From the comparison of the two figures, we can find that there are eight spikes in one period of the coaxial rotor thrust curve, while there are only four spikes in one period of the individual rotor thrust curve, and that the peak of fluctuation of the coaxial rotor thrust is larger than that of the individual rotor. For the coaxial rotors, the peak of fluctuation of the top rotor is a little larger than that of the bottom rotor. For the individual rotor helicopter model, only the fuselage has aerodynamic interactional influence on the rotor, so the appearance of the fluctuation of thrust is attributed to the aerodynamic interaction between the rotating rotor and the fuselage when the blades pass through the above region of the fuselage, taking no account of the possible influence of

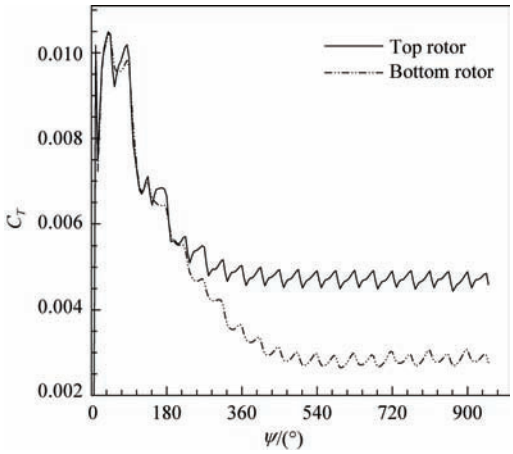

Fig.4 Thrust coefficient curves of coaxial rotors.

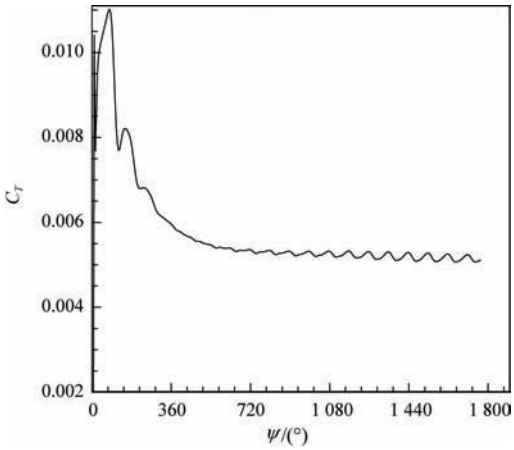

Fig.5 Thrust coefficient curve of individual rotor.

the asymmetric coming flow. However, for the coaxial rotor helicopter model, not only the fuselage has an influence on the rotor, but also the two coaxial rotors have strong aerodynamic interactional influence on each other, so the eight locations of the spikes are the encounter locations of the two coaxial rotors, because the rotor can encounter the other one for eight times in one rotating revolution. The larger fluctuating spike of the coaxial rotor thrust comparing to the individual rotor demonstrates that the aerodynamic interaction between the two coaxial rotors is much stronger than that between the rotor and fuselage. For the bottom rotor, the fluctuation of the thrust is the result of the collective effect of the interactions of both the top rotor and fuselage, and the fuselage's interaction influence on the bottom rotor is stronger than that on the top rotor due to a shorter distance from the bottom rotor to the fuselage, so the fluctuation spike of the bottom rotor thrust is smaller than that of the top rotor.

The comparison of downwash velocity w at the rotor planes on the longitudinal and lateral sectional planes respectively through the center of the rotor disk are given in Fig.6. The r denotes the radial distance from the center of rotor. The downwash velocity of the top rotor is a little larger than that of the individual rotor, and the downwash velocity of bottom rotor is much lagrer than that of the top rotor. This can be explained

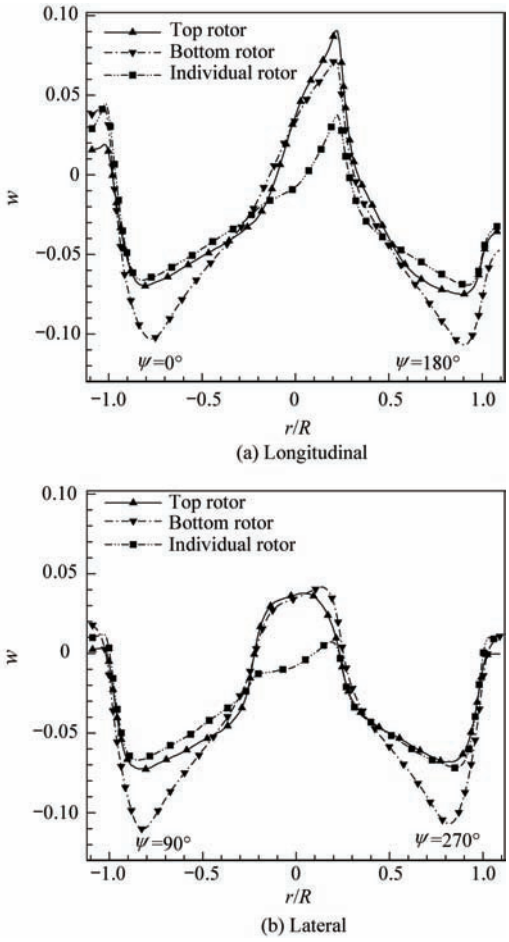

Fig.6 Comparison of downwash velocity.

as follows. The bottom rotor is located in the outflow of the top rotor, and the top rotor generates a large downwash velocity at the location of bottom rotor, adding the bottom rotor itself downwash, so the resulting collective downwash velocity at the location of bottom rotor plane is much larger than that of the individual rotor. On the other hand, the discrepancy of the downwash velocity can explain the difference of the thrust values between the two coaxial rotors in Fig.4. Larger downwash velocity decreases the effective angle of attack of the bottom rotor, resulting in a smaller thrust coefficient.

The spatial streamlines through the longitudinal mid-plane at the zero-azimuth-angle blade location are shown in Fig.7 for both the coaxial and individual rotor helicopter models. It is found that the flow around the coaxial rotor helicopter has a stronger downwash than the individual rotor helicopter, due to the larger thrust generated by the coaxial rotors, resulting in a stronger downwash flow.

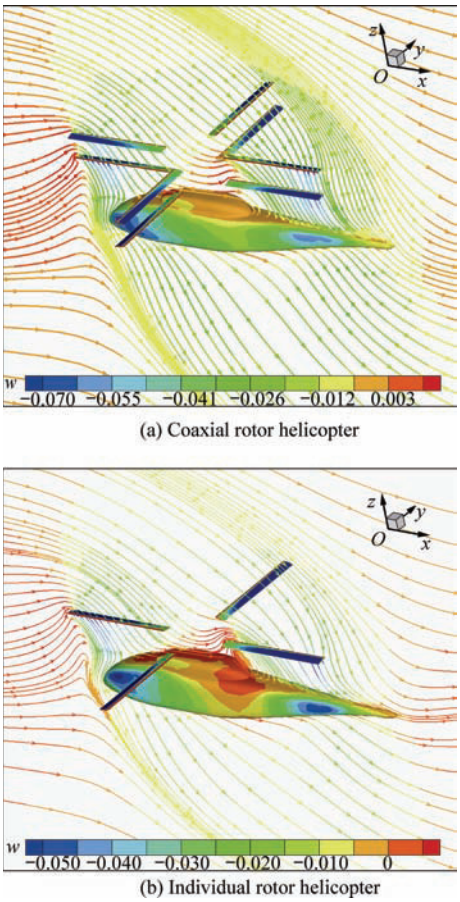

Fig.7 Streamlines on longitudinal mid-plane.

Fig.8 shows the iso-vorticity contours computed from the solution over the entire overset grids at a given instant. The figure shows the position of the rotor blades at that time level, and the vortices coming off the blades can be seen distinctly. The formation of the trailing tip vortex, its migration to the downstream of the rotor, and the impingement of the tip vortex on

the fuselage can be observed in the figure. The formation of the rotor disk vortex similar to the tip vortex of fixed wing is also clearly demonstrated.

Fig.8 Instantaneous iso-vorticity surface in the flowfield.

The surface streamlines on the fuselages of coaxial rotor helicopter and individual rotor helicopter are both shown in Fig.9 There are upwash vortex flows on the top of the fuselages, and the directions of the vortex are the same as the rotational directions of the bottom rotor and individual rotor respectively. It is found that the strength of the vortex of the coaxial rotor helicopter model is weaker than that of the individual rotor helicopter model, because the converse wake vortex induced by the top rotor decreases the strength of the vortex on the top of the fuselage. Additionally, the centers of the vortex of both models are behind the rotor shaft centers due to the streamwise component velocity of the coming flows.

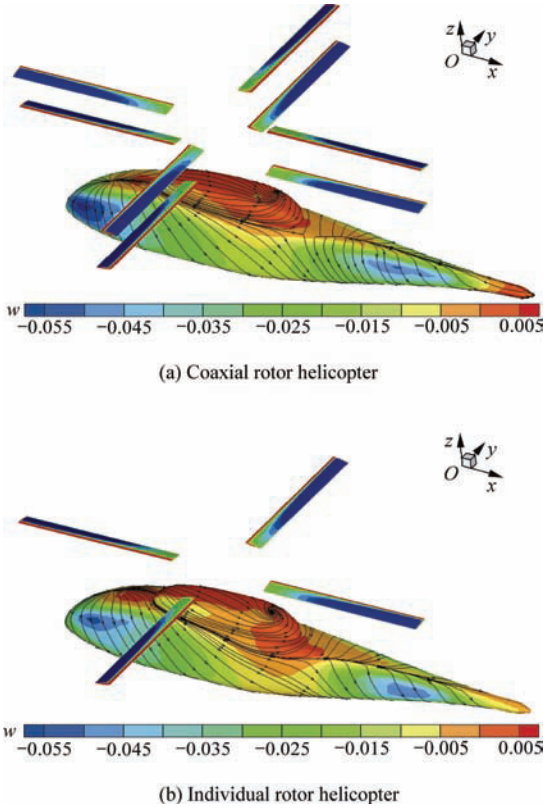

Fig.9 Surface streamlines on fuselages.

In order to investigate the influence of blade collective angle θ on the performance of forward flight coaxial rotor helicopter, the two models with blade collective angle of 12° are both simulated here, and the comparison with the cases of blade collective angle of 8° is given in Table 3.

Table 3 Comparison of thrust coefficients between different collective angles

Parameter	C_T			
	Top rotor	Bottom rotor	Summation	Individual rotor
θ=8°	0.004 7	0.002 9	0.007 6	0.005 1
θ=12°	0.007 8	0.005 7	0.013 5	0.008 6
Increment	0.003 1	0.002 8	0.005 9	0.003 5

From Table 3, we can find that the thrusts of coaxial rotors and individual rotor all increase when the collective angle of blade becomes larger. The increment of the top rotor is larger than that of the bottom rotor, and the increment of the individual rotor is a little larger than that of the top rotor.

Additionally, the influence of the rotor spacing on the performance of coaxial rotor helicopter is also investigated here by increasing the rotor spacing to 0.24 m, with the blade collective angle kept at 8°. The calculation results are shown in Table 4.

Table 4 Comparison of thrust coefficients between different rotor spacings

Parameter	C_T		
	Top rotor	Bottom rotor	Summation
H=0.16 m	0.004 70	0.002 90	0.007 60
H=0.24 m	0.004 75	0.002 65	0.007 40
Increment	0.000 05	−0.000 25	−0.000 20

From Table 4, we can find that when the rotor spacing becomes larger, the thrust coefficient of top rotor increases a little, but the thrust coefficient of bottom rotor decreases more, resulting in the total thrust coefficient reducing. The result of the comparison demonstrates that the aerodynamic interference of the bottom rotor on the top rotor decreases, while the interference of the top rotor on the bottom rotor is enhanced, with the resulting thrust reducing a little.

5. Conclusions

In the present article, the forward flight flows around the coaxial and individual rotor helicopters have been simulated by solving the three-dimensional unsteady Euler equations based on the unstructured dynamic overset grids, and some conclusions are obtained as follows.

(1) Compared to the individual rotor helicopter, the thrusts of both coaxial rotors are smaller; especially the thrust of bottom rotor is much smaller, which

demonstrates that the interaction between the coaxial rotors leads to decreasing the performance of the coaxial rotors, especially the bottom rotor.

(2) The interaction between the coaxial rotors makes the downwash velocity at the bottom rotor plane much larger than that at the individual rotor plane, and the downwash velocity at the top rotor plane is a little larger than that at the individual rotor plane.

(3) There are upwash vortex flows on the top of the fuselages of both helicopter models, and the strength of the coaxial rotor helicopter is weaker than that of the individual rotor helicopter.

(4) The downwash velocity and thrust coefficient both increase when the collective angle of blade becomes larger.

(5) When the rotor spacing increases, the thrust coefficients will increase for the top rotor and decrease for the bottom rotor, and the total thrust reduces a little.

It is demonstrated that the present method of unstructured dynamic overset grids is efficient and robust for simulating unsteady flows around helicopter with coaxial rotors, and new understandings of coaxial rotor systems and rotor/fuselage interactions will be studied in the future to uncover more aerodynamic problems of coaxial rotor systems.

References

[1] Andrew M J. Co-axial rotor aerodynamics in hover. Vertica 1981; 5(2):163-172.

[2] Saito S, Azuma A. A numerical approach to co-axial rotor aerodynamics. Vertica 1982; 6(3):253-266.

[3] Bagai A, Leishman J G. Free-wake analysis of tandem, tilt-rotor and co-axial rotor configurations. Journal of the American Helicopter Society 1996; 41(3):196-207.

[4] Leishman J G, Syal M. Figure of merit definition for coaxial rotors. Journal of the American Helicopter Society 2008; 53(3): 290-300.

[5] Leishman J G, Ananthan S. An optimum coaxial rotor system for axial flight. Journal of the American Helicopter Society 2008; 53(4): 366-381.

[6] Leishman J G. Aerodynamic performance considerations in the design of a coaxial proprotor. Journal of the American Helicopter Society 2009; 54(1): 012005-1-14.

[7] Lakshminarayan V K, Baeder J D. Computational investigation of micro-scale coaxial rotor aerodynamics in hover. Journal of Aircraft 2010; 47(3): 940-955.

[8] Lakshminarayan V K, Baeder J D. High resolution computational investigation of trimmed coaxial rotor aerodynamics in hover. Journal of the American Helicopter Society 2009; 54(4): 042008-1-21.

[9] Lakshminarayan V K, Baeder J D. Computational investigation of small scale coaxial rotor aerodynamics in hover. AIAA-2009-1069, 2009.

[10] Tong Z L, Sun M. Navier-Stokes calculations of coaxial rotor aerodynamics. Acta Aeronautica et Astronautica Sinica 1998; 19(1):1-5. [in Chinese]

[11] Kang N, Sun M. Navier-Stokes calculations of wake and ground vortex induced by a rotor in forward flight with ground effects. Acta Aeronautica et Astronautica Sinica 1996; 17(7):7-12. [in Chinese]

[12] Chen M, Hu J Z, Cao Y H. Rigid-wake analysis of rotor aerodynamics in forward flight. Journal of Beijing University of Aeronautics and Astronautics 2004; 30(1):74-78. [in Chinese]

[13] Deng Y M, Tao R, Hu J Z. Experimental investigation of the aerodynamic interaction between upper and lower rotors of a coaxial helicopter. Acta Aeronautica et Astronautica Sinica 2003; 24(1):10-14. [in Chinese]

[14] Huang S L, Xu G H, Li C H. Flow field analysis of coaxial twin rotors based on free wake. Journal of Nanjing University of Aeronautics and Astronautics 2008; 40(6):721-726. [in Chinese]

[15] Xu H Y, Ye Z Y. Numerical simulation of interaction unsteady flows around coaxial rotors. Journal of Aerospace Power 2011. [in Chinese] (in Press).

[16] Raymond E M, Gorton S A. Steady and periodic pressure measurements on a generic helicopter fuselage model in the presence of a rotor. NASA TM 2000-210286, 2000.

[17] Xu He Y, Ye Z Y, Wang G, et al. Improving numerical simulation of rotor forward flight flow field with unstructured dynamic overset grids. Journal of Northwestern Polytechnical University 2006; 24(6): 763-767. [in Chinese]

[18] Xu H Y, Ye Z Y, Wang G, et al. Simulation of helicopter forward flight flow using unstructured overset grids. AIAA-2009-1285, 2009.

[19] Gleize V, Pape A L. Low Mach number preconditioning for unsteady flow in general ALE formulation. AIAA-2006-687, 2006.

[20] Jameson A. Time dependent calculations using multigrid, with applications to unsteady flows past airfoils and wings. AIAA-1991-1596, 1991.

[21] Jameson A, Schmidt W, Turkel E. Numerical solutions of the Euler equations by finite volume methods using Runge-Kutta time stepping scheme. AIAA-1981-1259, 1981.

[22] Colin P C. A survey of theoretical and experimental coaxial rotor aerodynamic research. NASA TP 3675, 1997.

Biographies:

XU Heyong Born in 1980, he received B.S. and M.S. and Ph.D. degrees from Northwestern Polytechnical University in 2003, 2006 and 2009 respectively, and then did his post-doctoral research there. His main research interest is numerical simulation of unsteady flows using CFD methods.
E-mail: xhy2005@mail.nwpu.edu.cn

YE Zhengyin Born in 1963, he is a professor in Northwestern Polytechnical University. His main research interest lies in CFD and aeroelastic dynamics.
E-mail: yezy@nwpu.edu.cn